Solid Earth Discuss., 5, 365–390, 2013
www.solid-earth-discuss.net/5/365/2013/
doi:10.5194/sed-5-365-2013
© Author(s) 2013. CC Attribution 3.0 License.

Solid Earth
Discussions
Open Access

This discussion paper is/has been under review for the journal Solid Earth (SE).
Please refer to the corresponding final paper in SE if available.

The microstructural record of porphyroclasts and matrix of serpentinite mylonites – from brittle and crystal-plastic deformation to dissolution-precipitation creep

J. Bial[1] and C. A. Trepmann[2]

[1]Institut für Geowissenschaften, Abteilung Mineralogie – Petrologie, Universität Kiel, Ludewig-Meyn-Str. 10, 24098 Kiel, Germany
[2]Department für Geo- und Umweltwissenschaften, Ludwig-Maximilians-Universität München, Luisenstraße 37, 80333 München, Germany

Received: 19 March 2013 – Accepted: 20 March 2013 – Published: 12 April 2013

Correspondence to: J. Bial (jb@min.uni-kiel.de)

Published by Copernicus Publications on behalf of the European Geosciences Union.



Abstract

We examine the microfabric development in high-pressure, low-temperature metamorphic serpentinite mylonites exposed in the Erro-Tobbio Unit (Voltri Massif, Italy) using polarization microscopy and electron microscopy (SEM/EBSD, EMP). The mylonites are derived from mantle peridotites, were serpentinized at the ocean floor and underwent high pressure metamorphism during Alpine subduction. They contain diopside and olivine porphyroclasts embedded in a fine-grained matrix essentially consisting of antigorite. The porphyroclasts record brittle and crystal-plastic deformation of the original peridotites in the upper mantle at stresses of a few hundred MPa. After the peridotites became serpentinized, deformation occurred mainly by dissolution-precipitation creep resulting in a foliation with flattened olivine grains at phase boundaries with antigorite, crenulation cleavages and olivine and antigorite aggregates in strain shadows next to porphyroclasts. It is suggested that the fluid was provided by dehydration reactions of antigorite forming olivine and enstatite during subduction and prograde metamorphism. At sites of stress concentration around porphyroclasts antigorite reveals an associated SPO and CPO, characteristically varying grain sizes and sutured grain boundaries, indicating deformation by dislocation creep. Stresses were probably below a few tens of MPa in the serpentinites, which was not sufficiently high to allow for crystal-plastic deformation of olivine at conditions at which antigorite is stable. Accordingly, any intragranular deformation features of the newly precipitated olivine in strain shadows are absent.

The porphyroclast microstructures are not associated with the microstructures of the mylonitic matrix, but are inherited from an independent earlier deformation. The porphyroclasts record a high-stress deformation in the upper mantle of the oceanic lithosphere probably related to rifting processes, whereas the antigorite matrix records deformation at low stresses during subduction and exhumation.

SED
5, 365–390, 2013



1 Introduction

The exhumed HP-LT metamorphic mafic to ultramafic rocks from the Erro-Tobbio unit of the Voltri Massif, Italy, provide a unique record of the complex history through their disintegration from the mantle, uplift onto the ocean floor, subduction and exhumation (e.g. Vissers et al., 1991, 1995; Hoogerduijn Starting et al., 1993; Hermann et al., 2000; Healy et al., 2009). In this study, the microfabric development of mylonitic antigorite serpentinites is analysed in detail in order to elucidate the grain-scale deformation processes in the rocks that dramatically changed their mineral content and thus their rheological behaviour during the complex history. The aim is to differentiate between the potential record of independent successive deformation events. On the basis of the findings we discuss the implications for the inferred superposition of features associated with initial brittle and crystal-plastic deformation of the original mantle peridotites with features indicating dissolution-precipitation creep of the serpentinized peridotites together with evidence for localized dislocation creep of antigorite.

2 Geological setting of the Erro-Tobbio unit, Voltri Massif, Italy

The ophiolitic Voltri Massif is located in NW Italy, about 20 km NW of Genoa directly at the transition from the Ligurian Alps to the Apennine chain (Fig. 1). As largest ultramafic massif within the Alps–Apennine chain it is restricted eastward by the Sestri Voltaggio Zone and northward by the Piemont basin filled with Tertiary sediments (Hoogerduijn Strating et al., 1990). The peridotites from the Erro-Tobbio unit as part of the ophiolitic Voltri massif are interpreted to represent upper mantle rocks originating from the Mesozoic Piemont–Ligurian oceanic lithosphere, the Alpine-Apennine part of the Mesozoic Tethys (Hoogerduijn Strating et al., 1990). Shear zones in lherozolites from the Erro-Tobbio unit have been attributed to deformation processes during continental rifting (e.g. Drury et al., 1990; Vissers et al., 1991, 1995; Hoogerduijn Starting et al., 1993). The mantle peridotites are assumed to have been exhumed to shallow

SED
5, 365–390, 2013



lithospheric levels, where they became serpentinized (Bodinier et al., 1986; Scambelluri et al., 1997, 2004; Hermann et al., 2000).

During subduction of the Piemont–Ligurian ocean and Alpine collision, the Erro-Tobbio peridotites underwent an Alpine prograde metamorphism (Hoogerduijn Strating et al., 1990; Messiga et al., 1995; Scambelluri et al., 1995; Hermann et al., 2000). The peak metamorphic conditions of the Alpine metamorphism have been estimated at 1.8–2.5 GPa and 500–650 °C on the basis of the assemblage omphacite + chloritoid + garnet + zoisite ± talc in a mylonitic meta-gabbro by Messiga et al. (1995). This peak pressure condition indicates a subduction of the Erro-Tobbio unit up to 80 km depth (Hermann et al., 2000). Late Cretaceous ages between 80 and 100 Ma have been inferred for the HP-LT metamorphism on the basis of a comparison with data from the Western Alps (Hoogerduijn Strating et al., 1990) or Corsica (Cohen et al., 1981). Veins in antigorite serpentinites, containing olivine, titanian clinohumite, magnetite and diopside (Scambelluri et al., 1995) have been interpreted as dehydration cracks generated at HP-LT conditions and indicating the circulation of a free fluid phase (Hoogerduijn Strating and Vissers., 1991; Scambelluri et al., 2004; Healy et al., 2009). The prograde evolution of the Erro-Tobbio rocks is followed by a retrograde metamorphic history related to Alpine collision (Hoogerduijn Strating et al., 1990, Hoogerduijn Strating, 1994). The rocks are finally overprinted by a greenschist facies metamorphism (Hoogerduijn Strating, 1994) during Eocene to Oligocene between 30 and 40 Ma as estimated from calcschists in the Voltri massif (Hoogerduijn Strating et al., 1990). Brittle deformation occurs during Oligocene to Miocene indicated by breccias and conglomerates of late Eocene-Oligocene age (Hoogerduijn Strating et al., 1990). The antigorite serpentinites studied here, were collected in NW Italy about 10 km NW of Genova, SW of Mt. Poggio (44° 32.008′ N, 8° 46.666′ E) and SW of Mt. Tobbio (44° 31.817′ N, 8° 46.649′ E) in the Erro-Tobbio unit (Fig. 1).

SED
5, 365–390, 2013



3 Methods

Specimens collected in the field were cut in two directions normal to the foliation (normal and parallel to the lineation) and polished thin sections with a thickness of ca. 30 µm were prepared. The thin sections were examined with a polarization microscope and analysed with the electron backscattered diffraction (EBSD)-method (Prior et al. 1996, 1999) using the scanning electron microscope (SEM) LEO 1530 at the Ruhr-University, Bochum. For EBSD investigations, mechanically polished thin sections have additionally been chemically polished with Syton® for 15 min to reduce surface damage and then coated with carbon to avoid charging effects. For the EBSD analysis the thin sections were tilted at an angle of 70° with respect to the beam and an accelerating voltage of 20 kV and a working distance to 25 µm was used. The EBSD-data were analysed using the Oxford Instruments HKL-software CHANNEL 5. A CAMECA SX-50 electron microprobe was used for the analysis of the chemical mineral composition.

4 Sample description and microfabrics

The investigated serpentinites are characterized by the mineral paragenesis olivine + diopside + antigorite + spinel + chlorite ± titanian clinohumite ± enstatite. The modal composition is strongly varying but typically in the range of 46–51 % antigorite, 10–20 % olivine, 5–10 % diopside, 5–7 % chlorite, 2–3 % spinel, 0–2 % enstatite. All investigated serpentinites show a pervasive foliation. In thin sections, the foliation is defined by antigorite-rich layers with a shape preferred orientation (SPO) of the grains. Antigorite forms a matrix in which large isolated olivine and diopside porphyroclasts are embedded (Fig. 2).

The olivine porphyroclasts have an average grain diameter of 1.2 mm (Fig. 2). They show undulatory extinction, deformation bands, low angle grain boundaries (LAGBs) forming chess-board-like patterns and irregular subgrains (Fig. 3a–c). Olivine

SED
5, 365–390, 2013



porphyroclasts are partly recrystallised. The new grains occur in intragranular bands (Fig. 3c, d) or along the boundary of porphyroclasts (Fig. 3e, f). The size of the recrystallised grains is typically in the range of 10–50 µm. The boundaries of recrystallised grains are smoothly curved and even. The new grains are not showing undulatory extinction or other substructures. Low-angle grain boundaries in the porphyroclasts (Fig. 4a) show a similar isometric shape and size as compared to the new grains. The crystallographic orientation of the new grains scatters around the crystallographic orientation of the host (Fig. 4c, d). The olivine porphyroclasts consist of $Fo_{90–87}$ with an average composition of $Mg_{1.8}Fe_{0.2}SiO_4$. In comparison, recrystallised grains have a lower X_{Mg} with an average composition of $Mg_{1.7}Fe_{0.3}SiO_4$ in the range of $Fo_{87–85}$ (Fig. 5). No chemical zoning in single grains is apparent (Fig. 5). Some of the olivine porphyroclasts embedded in the antigorite matrix show asymmetric strain shadows (Fig. 2), in which fine-grained olivine (20–40 µm in diameter) and antigorite aggregates (Fig. 6b, c) occur. In these aggregates antigorite grains are elongate (long axis: 200–400 µm) and show rare grain boundaries. Instead, phase boundaries to fine-grained olivine dominate (Fig. 6c). The size of the olivine grains in the strain shadow ranges from 5 to 60 µm. Their composition is with $Fo_{82–86}$ lower in Mg compared to recrystallised olivine and olivine porphyroclasts. Olivine and antigorite grains in strain shadows show a SPO by a preferred 2-D-orientation of the long axis parallel to the foliation of the sample (Fig. 6c, f). Whereas the SPO is associated with a crystallographic preferred orientation (CPO) for antigorite with the (001) basal plane in the foliation plane, olivine grains show no marked CPO (Fig. 6c, e).

Large diopside porphyroclasts occur in the serpentinite mylonites embedded in the antigorite matrix with an average grain diameter of ca. 2 mm. (Figs. 2, 7). The average composition is $(Mg_{0.9}, Fe_{0.1}, Ca_{0.9}, Al_{0.1})$ $[(Si_{1.9}, Al_{0.1})O_6]$. All diopside porphyroclasts show exsolution lamellae parallel (100) with a relative constant spacing and a width of a few µm (Fig. 7), are commonly fractured (Fig. 7a), kinked and bent (Fig. 7b, c). The stereographic projection of bent crystals shows that the orientation of the [010] is a common axis and thus probably representing the rotation axis (i.e. the normal to the

SED
5, 365–390, 2013



glide direction within the glide plane) during glide-controlled deformation. The relative misorientation at the kink bands is high with approximately 50°–70° (Fig. 7). Also in kink bands, the [010] axis is the common axis. In strain shadows around diopside porphyroclasts, aggregates of diopside and enstatite occur (Fig. 6a). The new pyroxene crystals in the strain shadows do not show any exsolution lamellae, in contrast to the porphyroclasts.

Antigorite is occurring as long needles growing into olivine porphyroclasts (Figs. 3–5, 8a), together with olivine in strain shadows (Fig. 6b, c) and in almost monomineralic antigorite layers (Fig. 8). Fine-grained olivine can be enriched in small-scaled fold hinges and short limbs of asymmetric antigorite-rich multilayers forming a crenualtion cleavage (Fig. 8a, b). The pronounced SPO of antigorite corresponds to a CPO with the (001) basal plane in the foliation plane (Fig. 8). The size of antigorite grains that show sutured grain boundaries is strongly varying in the vicinity of porphyroclasts at sites of stress concentrations, where also the CPO is deflected (Fig. 8c, d).

5 Discussion

5.1 Deformation of olivine and diopside porphyroclasts

The deformed diopside porphyroclasts (Fig. 7) record brittle and crystal-plastic deformation by dislocation glide. The bent (100) plane, the common rotation axis and kink band axis parallel to [010] indicate that the glide system (100) [001] was active. The intragranular deformation microstructures in olivine porphyroclasts (undulatory extinction, deformation bands, LAGBs) indicate inhomogeneous crystal-plastic deformation with dislocation glide and climb (Fig. 3). The intragranular zones with recrystallised small grains show a crystallographic orientation similar to that of the host porphyroclast. The porphyroclasts show many subgrains (Fig. 4) with a similar size and shape compared to the recrystallised grains (Figs. 3c–f, 4, 5). Both observations suggest subgrain rotation recrystallisation in the regime of dislocation creep, where the new

SED
5, 365–390, 2013



grains inherit a crystallographic orientation similar to that of the replaced original grain (e.g. Nicolas and Poirier, 1976; Poirier, 1985; Urai et al., 1986; Drury and Urai, 1990; Lloyd and Freeman, 1994; Bestmann and Prior, 2003; Trepmann and Stöckhert, 2009). Growth of new grains along former microcracks, is suggested by intragranular zones of recrystallised grains that show a systematic chemical variation to the host porphyroclast. The different chemical composition of olivine porphyroclasts and intragranular new grains indicate the involvement of chemical reactions during recrystallisation. A secondary chemical variation caused by the larger surface area in relation to the grain volume of the recrystallised grains seems unlikely, as the porphyroclasts do not show any chemical variation at their phase boundary to the antigorite matrix. Chemical reactions during dislocation creep are known to be able to cause chemical variation of recrystallised grains (e.g. Yund and Tullis, 1991; Stünitz, 1998; Büttner and Kasemann, 2007). The observed decrease in the X_{Mg} values in intragranular recrystallised zones requires an exchange reaction between olivine and a co-existing solid or fluid phase, both being favoured by the presence of a circulating free fluid.

The absence of serpentine minerals in the intragranular recrystallised olivine aggregates within olivine porphyroclasts implies temperatures higher than 600 °C (e.g. Hermann et al., 2000; Scambelluri et al., 2004) during recrystallisation. A temperature above 600 °C is also in accord with the general assumption that dynamic recrystallisation of olivine in the regime of dislocation creep at reasonable strain rates of 10^{-13}–10^{-15} s^{-1} requires temperatures considerably higher than 600 °C as based on observations from natural systems (e.g. Skrotzki et al., 1990; Altenberger, 1995; Jin et al., 1998) and the extrapolation from experimentally derived flow laws (Fig. 9, Chopra and Paterson, 1981; Hirth and Kohlstedt, 2003). The recrystallisation grain size paleopiezometers of van der Wal et al. (1993) for the observed recrystallised grain sizes of 10–50 µm would indicate differential stresses on the order 70–250 MPa. Assuming that an extrapolation of the experimentally derived flow law to relevant strain rates of 10^{-13}–10^{-15} s^{-1} is valid and that the grain size paleopiezometer is applicable, temperature conditions of 650–800 °C are thus indicated for dynamic recrystallisation. However, it is not excluded,

SED
5, 365–390, 2013



but rather likely, that stresses and strain rates have been higher at an early stage of dislocation glide-controlled deformation associated with brittle deformation, recorded by the fractured, kinked and bent diopside porphyroclasts and intragranular recrystallised zones in deformed olivine porphyroclasts. Localized intragranular zones of recrystallised grains within deformed porphyroclasts suggest that recrystallisation was restricted at sites of high strain, e.g. along former fractures, kink bands and deformation bands. Such deformation features have been observed from naturally deformed peridotites from the Balmuccia complex in the Western Alps (Matysiak and Trepmann, 2012) and by deformation and annealing experiments on peridotites (Druiventak et al., 2012). Intragranular zones of recrystallised grains within deformed porphyroclasts are indicators for a switch from an initial brittle and glide-controlled deformation in the low-plasticity regime followed by dislocation creep. Such a microstructural development is characteristic for stress variations at the lower tip of seismically active fault zones (Trepmann and Stöckhert, 2003; Trepmann et al., 2007; Druiventak et al., 2012; Matysiak and Trepmann, 2012). However, the chemical variance of recrystallised grains and host porphyroclasts observed here is in contrast to the remarkably homogeneous chemical composition of the localized recrystallised grains and porphyroclasts in peridotites from the Ivrea zone (Matysiak and Trepmann, 2012).

5.2 Deformation of serpentinite

The fine-grained aggregates of olivine and antigorite in strain shadows (Fig. 6b, c) around olivine and diopside porphyroclasts indicate that they were precipitated from the pore fluid during deformation. In almost monomineralic antigorite layers with the (001) basal plane of antigorite parallel to the foliation, fine-grained olivine can be enriched in asymmetric multilayer folds (Fig. 8a, b). This indicates that either olivine crystallized during folding from the pore fluid, possibly on the expense of antigorite, or that olivine was present before folding and was redistributed by dissolution along the phase boundaries to antigorite. The microstructure in the strain shadows as well as the crenulation cleavage indicate that the phase boundaries between antigorite and olivine act

SED
5, 365–390, 2013



as sites of preferred dissolution during deformation by dissolution-precipitation creep (Wassmann et al., 2011).

In monomineralic antigorite aggregates, a characteristic grain size variation with fine-grained antigorite at sites of stress concentrations showing a marked CPO around porphyroclasts and sutured grain boundaries (Fig. 8c, d) point to deformation by dislocation creep. The lack of undulatory extinction, LAGBs and subgrains in newly precipitated olivine and pyroxene grains indicates differential stresses insufficiently high for crystal-plastic deformation of olivine and pyroxene at conditions at which antigorite is stable. Consistently, the flow law for dislocation creep of antigorite derived by Hilairet et al. (2007) would indicate differential stresses on the order of 5 MPa assuming a strain rate of $10^{-14}\,s^{-1}$ and 50 MPa for a strain rate of $10^{-10}\,s^{-1}$.

6 Implications

The deformation microstructures of the porphyroclasts are interpreted to have developed in the original mantle peridotite before hydration of the peridotite and transformation into serpentinite mylonites – at upper mantle temperature conditions (650–800 °C, i.e. considerably higher than suggested for the Alpine HP-LT metamorphism) and differential stresses of a few hundred MPa. Similar deformation features formed at upper mantle conditions are described in peridotite mylonites from the Erro-Tobbio unit and have been related to Jurassic rifting (Vissers et al., 1991; Hoogerduijn Starting et al., 1993). Rifting processes are known to be associated with deep earthquakes (e.g. Albaric et al., 2009, 2010; Ibs-von Seht et al., 2008). At the lower tip of seismically active fault zones peridotites can be affected by a sequence of high-stress deformation followed by recrystallisation at decreasing stresses (Druiventak et al., 2011, 2012; Matysiak and Trepmann, 2012), consistent with the microstructural record of the porphyroclasts.

The deformed mantle peridotites were uplifted and transformed to a serpentine-rich mineralogy by low grade hydration near the ocean floor (Scambelluri et al., 1997).

SED
5, 365–390, 2013



The serpentinites were subsequently subducted during Alpine collision (Hoogerduijn Strating et al., 1990; Messiga et al., 1995; Scambelluri et al., 1995; Hermann et al., 2000). Dehydration reactions of antigorite according to the reactions

$$\text{Antigorite} + \text{Brucite} \rightarrow \text{Olivine} + \text{Water} \quad (1)$$

$$\text{Antigorite} \rightarrow \text{Olivine} + \text{Enstatite} + \text{Water} \quad (2)$$

have been proposed to be recorded by the HP-LT metamorphic mineral assemblage of the Erro-Tobbio serpentinites (Hoogerduijn Strating and Vissers, 1991; Scambelluri et al., 1991, 2004; Ulmer and Trommsdorff, 1995; Hermann et al., 2000; Healey et al., 2009). These antigorite breakdown reactions can provide a considerable amount of fluid to depth of up to 200 km (Ulmer and Trommsdorff, 1995; Bromiley and Pawley, 2003; Scambelluri et al., 2004).

The observed secondary olivine and enstatite crystals occurring in strain shadows of diopside and olivine porphyroclasts (Fig. 6) as well as olivine in foliated antigorite aggregates (Fig. 8a, b) are assumed to have formed by these reactions and during deformation by dissolution-precipitation creep during alpine subduction and exhumation. The dehydration reactions provided the fluids for effective dissolution-precipitation creep at stresses below a few tens of MPa, as indicated by evidence for dislocation creep in monomineralic aggregates of antigorite on the one hand and undeformed newly precipitated olivine in strain shadows on the other.

It is remarkable that the deformed and recrystallised microstructure of the peridotites is partly preserved and not more effectively modified by serpentinization. This leads to the assumption that the serpentinized parts of the microstructure were areas of even higher strain (e.g. shear zones with recrystallised areas of finer grain sizes) than the preserved relicts. Thus, the porphyroclasts record the minimum strain of an independent deformation event not related to the mylonitic antigorite matrix.

SED
5, 365–390, 2013



7 Summary and conclusions

The microfabrics of the serpentinite mylonites record the changing rheological behaviour during their complex geological history with a dramatic change in mineral composition from original mantle peridotite to HP-LT metamorphic serpentinites. Based on our observations the following is inferred:

1. Brittle and crystal-plastic deformation of olivine and diopside occurred in peridotites, leading to undulatory extinction, deformation bands and intragranular recrystallised areas in olivine porphyroclasts and fragmented and kinked diopside porphyroclasts. The deformation took place at upper mantle conditions and differential stresses of few hundred MPa. Chemical reactions during dislocation creep probably in the presence of a pore fluid are indicated by a different chemical composition of recrystallised olivine and olivine porphyroclasts. A likely geological situation for the recorded deformation is the deep area of a nearby seismically active mantle shear zone probably related to Jurassic rifting.

2. Antigorite breakdown reactions together with dissolution-precipitation creep lead to the foliation of the serpentinite mylonites, formation of strain shadows and crenulation cleavages with growth of new olivine and pyroxene. Deformation by dissolution-precipitation creep took place during alpine subduction and exhumation. Simultaneously, in monomineralic antigorite aggregates, dislocation creep is indicated by sutured grain boundaries, characteristic grain size variations and a deflected combined SPO and CPO at sites of stress concentrations. Undeformed newly precipitated olivine indicates that stress conditions remained since then insufficiently high for crystal-plastic deformation of olivine at conditions at which antigorite is stable, i.e. below a few tens of MPa.

The internal deformation of the olivine and pyroxene porphyroclasts is not associated with the matrix deformation in the serpentinite mylonites but is inherited and records an independent earlier deformation event. The serpentinite mylonites investigated here

SED
5, 365–390, 2013



are an example, that the microstructural record of porphyroclasts in mylonites does not necessarily correspond to that of the mylonitic matrix but can provide information on an earlier deformation event in the geological history of the protholith.

Acknowledgements. We thank Bernhard Stöckhert for many stimulating discussions and constructive criticism on an earlier draft of the manuscript. Financial support by the German Science Foundation within the scope of Collaborative Research Centre 526 "Rheology of the Earth" is gratefully acknowledged.

References

Albaric, J., Déverchère, J., Petit, C., Perrot, J., and Le Gall, B.: Crustal rheology and depth distribution of earthquakes: insights from the central and southern East African Rift System, Tectonophysics, 468, 28–41, doi:10.1016/j.tecto.2008.05.021, 2009.

Albaric, J., Perrot, J., Déverchère J., Deschamps, A., Le Gall, B., Ferdinand, R. W., Petit, C., Tiberi, C., Sue, C., and Songo, M.: Contrasted seismogenic and rheological behaviours from shallow and deep earthquake sequences in the North Tanzanian Divergence, East Africa, J. Afr. Earth Sci., 58, 799–811, doi:10.1016/j.jafrearsci.2009.09.005, 2010.

Altenberger, U.: Long-term deformation and fluid-enhanced mass transport in a Variscan peridotite shear zone in the Ivrea Zone, northern Italy: a microtextural, petrological and geochemical study of a reactivated shear zone, Int. J. Earth. Sci., 84, 591–606, 1995.

Bestmann, M. and Prior, D. J.: Intragranular dynamic recrystallization in naturally deformed calcite marble: diffusion accommodated grain boundary sliding as a result of subgrain rotation recrystallization, J. Struct. Geol., 25, 1597–1613, doi:10.1016/S0191-8141(03)00006-3, 2003.

Bodinier, J. L., Guiraud, M., Dupuy, C., and Dostal, J.: Geochemistry of basic dykes in the Lanzo Massif (W. A.), Tectonophysics, 128, 77–95, 1986.

Bromiley, G. D. and Pawley, A.: The stability of antigorite in the system MgO-SiO_2-H_2O (MSH) and MgO-Al_2O_3-SiO_2-H_2O (MASH): the effect of Al_3^+ substitution on high-pressure stability, Am. Mineral., 88, 99–108, 2003.

Büttner, S. H. and Kasemann, S. A.: Deformation-controlled cation diffusion in tourmaline: a microanalytical study on trace elements and boron isotopes, Am. Mineral., 92, 1862–1874, doi:10.2138/am.2007.2567, 2007.

SED
5, 365–390, 2013



Cohen, C. R., Schweickert, R. A., and Odom, A. L.: Age of emplacement of the Schists Lustrés nappe, Alpine Corsica, Tectonophysics, 73, 276–284, 1981.
Chopra, P. N. and Paterson, M. S.: The experimental deformation of dunite, Tectonophysics, 78, 453–476, 1981.
Druiventak, A., Trepmann, C. A., Renner, J., and Hanke, K.: Low-temperature plasticity of olivine during high stress deformation of peridotite at lithospheric conditions; an experimental study, Earth Planet. Sc. Lett., 311, 199–211, doi:10.1016/j.epsl.2011.09.022, 2011.
Druiventak, A., Matysiak, A., Renner, J., and Trepmann, C. A.: Kick-and-cook experiments on peridotite; simulating coseismic deformation and post-seismic creep, Terra Nova, 24, 62–69, doi:10.1111/j.1365-3121.2011.01038.x, 2012.
Drury, M. R. and Urai, J. L.: Deformation-related recrystallisation process, Tectonophysics, 172, 235–253, 1990.
Healy, D., Reddy, S. M., Timms, N. E., Gray, E. M., and Brovarone, A. V.: Trench-parallel fast axes of seismic anisotropy due to fluid-filled cracks in subducting slabs, Earth Planet. Sc. Lett., 283, 75–86, doi:10.1016/j.epsl.2009.03.037, 2009.
Hermann, J., Müntener, O., and Scambelluri, M.: The importance of serpentinite mylonites for subduction and exhumation of oceanic crust, Tectonophysics, 327, 225–238, 2000.
Hilairet, N., Reynard, B., Wang, Y., Daniel, I., Merkel, S., Nishiyama, N., and Petitgirard, S.: High-pressure creep of serpentinite, interseismic deformation, and initiation of subduction, Science, 318, 1910–1913, doi:10.1126/science.1148494, 2007.
Hirth, G. and Kohlstedt, D.: Rheology of the upper mantle and the mantle wedge: a view from the experimentalists, in: The Subduction Factory, edited by: Eiler, J., Geoph. Monogr. Series, American Geophysical Union, 138, 83–105, 2003.
Hoogerduijn Strating, E. H.: Extensional faulting in an intraoceanic subduction complex – working hypothesis for the Palaeogene of the Alps – Apennine system, Tectonophysics, 238, 255–273, 1994.
Hoogerduijn Strating, E. H. and Vissers, R. L. M.: Dehydration-induced fracturing of eclogite-facies peridotites: implications for the mechanical behavior of subducting oceanic lithosphere, Tectonophysics, 200, 187–198, 1991.
Hoogerduijn Strating, E. H., Piccardo, G. B., Rampone, E. Scambelluri, M., and Vissers, R. L. M.: The structure and petrology of the Erro-Tobbio peridotite, Voltri massif, Ligurian alps, guidebook for a two-day-excursion with emphasis on processes in the upper mantle (Voltri Massif, 26–28 June 1989), Ofioliti, 15, 119–184, 1990.

SED
5, 365–390, 2013



Hoogerduijn Strating, E. H., Rampone, E., Piccardo, G. B., Drury, M. G., and Vissers, R. L. M.: Subsolidus emplacement of mantle peridotites during incipient oceanic rifting and opening of the Mesozoic Tethys (Voltri Massif, NW Italy), J. Petrol., 34, 901–927, 1993.

Ibs-von Seht, M., Plenefisch, T., and Klinge, K.: Earthquake swarms in continental rifts – a comparison of selected cases in America, Africa and Europe, Tectonophysics, 452, 66–77, doi:10.1016/j.tecto.2008.02.008, 2008.

Jin, D., Karato, S.-I., and Obata S-I.: Mechanisms of shear localization in the continental lithosphere: inference from the deformation microstructures of peridotites from the Ivrea zone, northwestern Italy, J. Struct. Geol., 20, 195–209, 1998.

Lloyd, G. E. and Freeman, B.: Dynamic recrystallization of quartz under greenschist consitions, J. Struct. Geol., 16, 867–881, 1994.

Matysiak, A. K. and Trepmann, C. A.: Crystal-plastic deformation and recrystallization of peridotite controlled by the seismic cycle, Tectonophysics, 530–531, 111–127, doi:10.1016/j.tecto.2011.11.029, 2012.

Messiga, B., Scambelluri, M., and Piccardo, G. B.: Chloritoid-bearing assemblages in mafic systems and eclogite-facies hydration of alpine Mg-Al metagabbros (Erro-Tobbio Unit, Ligurian Western Alps), Eur. J. Mineral., 7, 1149–1167, 1995.

Nicolas, A. and Poirier, J. P.: Crystalline Plasticity and Solid State Flow in Metamorphic Rocks, John Wiley and Sons, London, 444 pp., 1976.

Poirier, J.-P.: Creep of Crystals – High Temperature Deformation Processes in Metals, Ceramics and Minerals, Cambridge University press, Cambridge, 260 pp., 1985.

Prior, D. J., Trimby, P. W., Weber, U. D., and Dingley, D. J.: Orientation contrast imaging of microstructures in rocks using forescatter detectors in the scanning electron microscope, Mineral. Mag., 60, 859–869, 1996.

Prior, D. J., Boyle, A. P., Brenker, F., Cheadle, M. C., Day, A., Lopez, G., Peruzzi, L., Potts, G., Reddy, S., Spiess, R., Timms, N. E., Trimby, P., Wheeler, J., and Zetterstrom, L.: The application of electron backscatter diffraction and orientation contrast imaging in the SEM to textural problems in rocks, Am. Mineral., 84, 1741–1759, 1999.

Scambelluri, M., Hoogerduijn Strating, E. H., Piccardo, G. B., Vissers, R. L. M., and Rampone, E.: Alpine olivine- and titanian clinohumite-bearing assemblages in the Erro-Tobbio peridotite (Voltri Massif, NW Italy), J. metamorph. Geol., 9, 79–91, 1991.

Scambelluri, M., Müntener, O., Hermann, J., Piccardo, G. B., and Trommsdorff, V.: Subduction of water into mantle: history of an Alpine peridotite, Geology, 23, 459–462, 1995.

SED
5, 365–390, 2013



Scambelluri, M., Piccardo, G. B., Philippot, P., Robbiano, A., and Negretti, L.: High salinity fluid inclusion formed from recycled seawater in deeply subducted alpine serpentinite, Earth Planet. Sc. Lett., 148, 485–499, 1997.

Scambelluri, M., Müntener, O., Ottolini, L., Pettke, T. T., and Vannucci, R.: The fate of B, Cl and Li in the subducted oceanic mantle and in the antigorite breakdown fluids, Earth Planet. Sc. Lett., 222, 217–234, doi:10.1016/j.epsl.2004.02.012, 2004.

Skrotzki, W., Wedel, A., Weber, K., and Müller, W. F.: Microstructure and texture in lherzolites of the Balmuccia massif and their significance regarding the thermomechanical history, Tectonophysics, 179, 227–251, 1990.

Stünitz, H.: Syndeformational recrystallization ± dynamic or compositionally induced?, Contrib. Mineral. Petrol., 131, 219–236, 1998.

Trepmann, C. A. and Stöckhert, B.: Quartz microstructures developed during non-steady state plastic flow at rapidly decaying stress and strain rate, J. Struct. Geol., 25, 2035–2051, doi:10.1016/S0191-8141(03)00073-7, 2003.

Trepmann, C. A. and Stöckhert, B.: Microfabric of folded quartz veins in metagreywackes: dislocation creep and subgrain rotation at high stress, J. metamorph. Geol., 27, 555–570, doi:10.1111/j.1525-1314.2009.00842.x, 2009.

Trepmann, C. A., Stöckhert, B., Dorner, D., Moghadam, R. H., Küster, M., and Röller, K.: Simulating coseismic deformation of quartz in the middle crust and fabric evolution during postseismic stress relaxation; an experimental study, Tectonophysics, 442, 83–104, doi:10.1016/j.tecto.2007.05.005, 2007.

Ulmer, P. and Trommsdorff, V.: Serpentine stability to mantle depths and subduction-related magmatism, Science, 268, 858–861, 1995.

Urai, J. L., Means, W. D., and Lister, G. S.: Dynamic recrystallization of minerals, Geoph. Monogr. Series, 36, 161–199, 1986.

Van der Wal, D., Chopra, P., Drury, M., and Fitz Gerald, J.: Relationship between dynamic recrystallized grain size and deformation conditions in experimentally deformed olivine rocks, Geophys. Res. Lett., 20, 1479–1482, 1993.

Vissers, R. L. M., Drury, M. R., Hoogerduijn Strating, E. H., and van der Wal, D.: Shear zones in the upper mantle – a case study in an Alpine lherzolite massif, Geology, 19, 990–993, 1991.

Vissers, R. L. M., Drury, M. R., Hoogerduijn Strating, E. H., Spiers, C. J., and van der Wal, D.: Mantle shear zones and their effect on lithosphere strength during coninental breakup, Tectonophysics, 249, 155–171, 1995.

SED
5, 365–390, 2013



Wassmann, S., Stöckhert, B., and Trepmann, C. A.: Dissolution precipitation creep versus crystalline plasticity in high pressure metamorphic serpentinites, Geol. Soc., London, Special Publications, 360, 129–149, 2011.

Yund, R. A. and Tullis, J.: Compositional changes of minerals associated with dynamic recrystallization, Contrib. Mineral. Petrol., 108, 346–355, 1991.

SED
5, 365–390, 2013



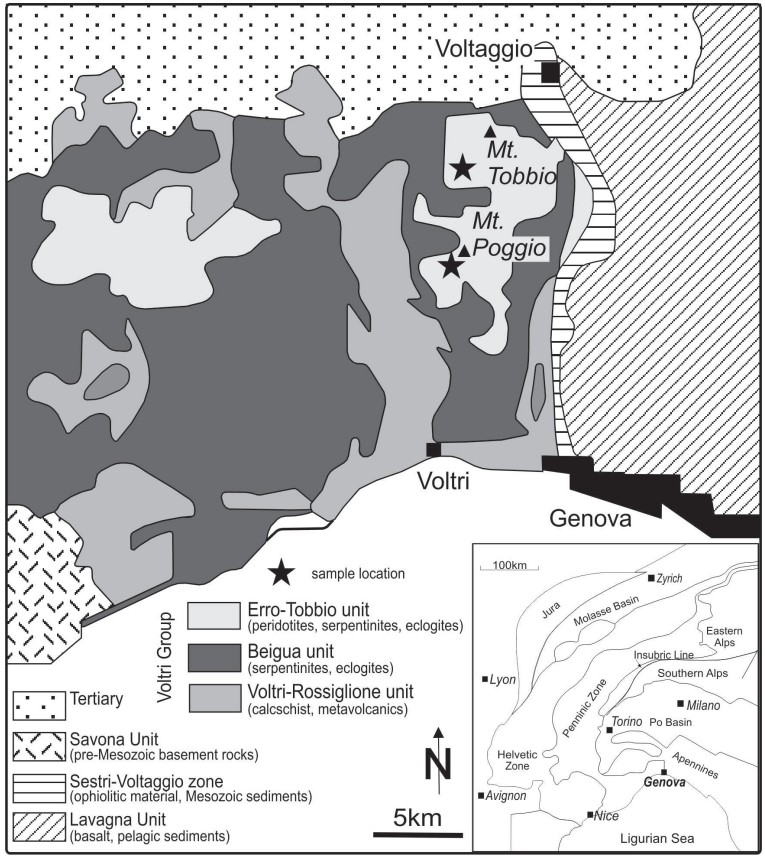


Fig. 1. Schematic tectonic map of the Voltri Group (after Scambelluri et al., 1991). Serpentinites have been sampled from the Erro-Tobbio unit close to Mt. Tobbio and Mt. Poggio.

SED
5, 365–390, 2013



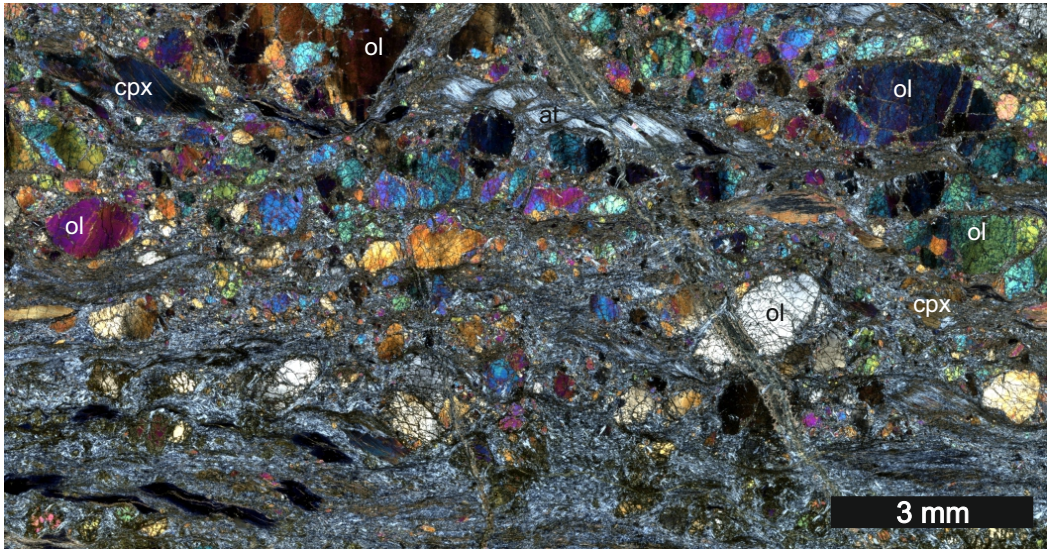


Fig. 2. Micrograph (crossed polarizers) of a typical sample of investigated serpentinite mylonites. Olivine and clinopyroxene porphyroclasts are embedded in an antigorite-rich matrix (sample CT_07-13).

SED
5, 365–390, 2013



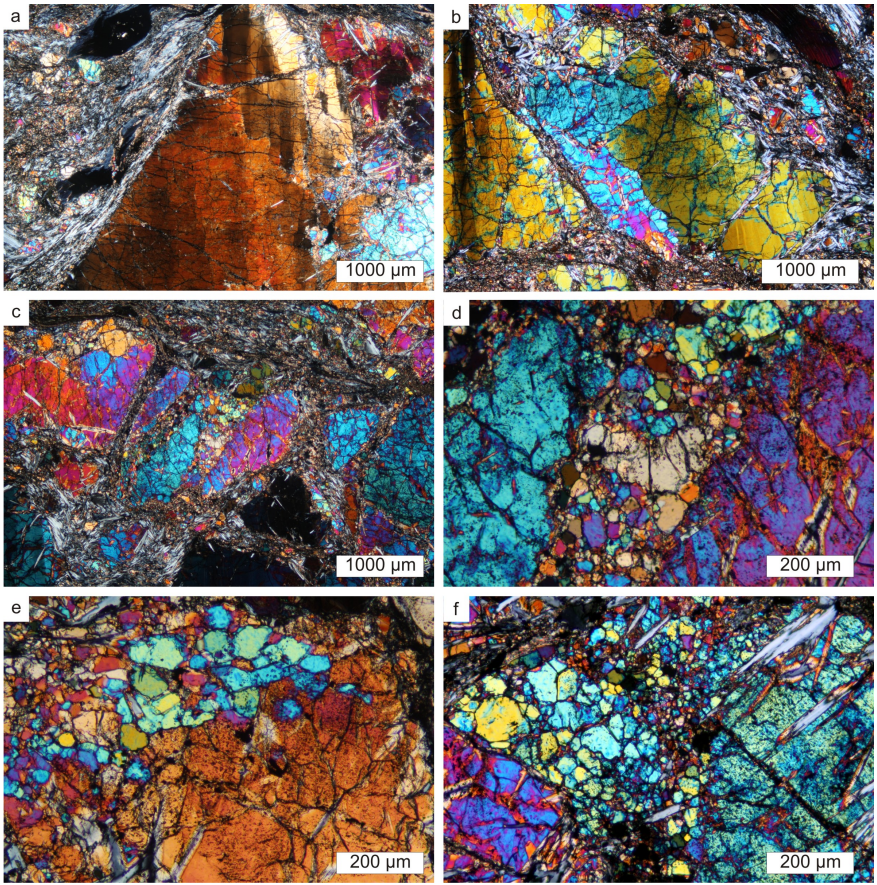


Fig. 3. Optical micrographs (crossed polarizers) showing microstructures in olivine porphyroclasts from sample CT_07-13. **(a, b)** Deformation bands and subgrains in olivine porphyroclasts; **(c, d)** Intragranular zones of recrystallised olivine grains within olivine porphyroclast; **(e, f)** Partly recrystallised olivine porphyroclasts. EBSD map of area in f is presented in Fig. 4.

SED
5, 365–390, 2013



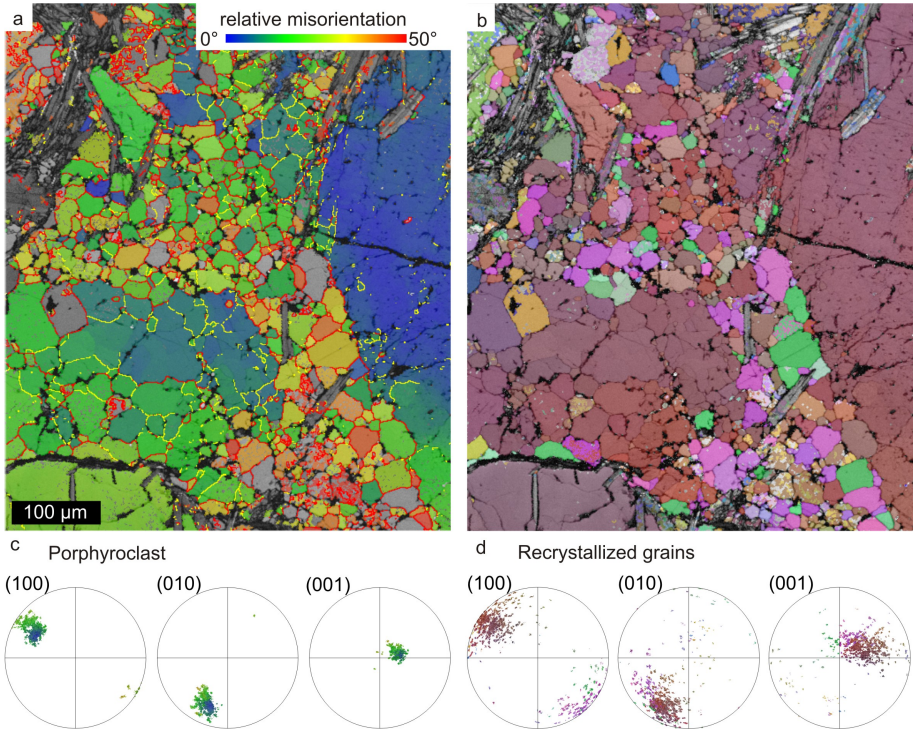


Fig. 4. EBSD data presented as maps showing the relative misorientation **(a)** and colour coded by the three Euler angles **(b)** of a partly recrystallised olivine porphyroclast (sample CT_07-13, compare Fig. 3f). Yellow lines in **(a)** represent low angle grain boundaries (misorientation < 10°), red lines represent high angle grain boundaries (misorientation > 10°). **(c, d)** Corresponding polefigures of poles to (100), (010) and (001) planes in an equal angle projection of the lower hemisphere for porphyroclasts and recrystallised grains, respectively.

SED
5, 365–390, 2013



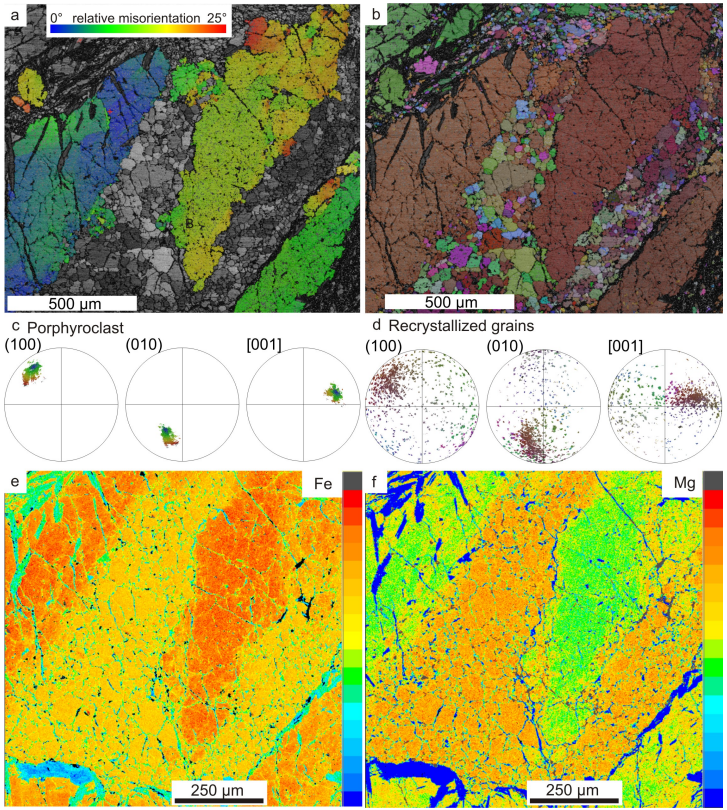


Fig. 5. (a, b) EBSD maps of partly recrystallised olivine porphyroclast (sample CT_07-13) showing relative misorientation and colour coded by three Euler angles, respectively. **(c, d)** Polefigures of poles to (100), (010) and (001) planes (equal angle projection, lower hemisphere). **(e, f)** EMP maps of the same area with relative distribution of Fe **(e)** and Mg **(f)** (red: high content, blue: low content) showing a systematic difference of a more Fe-rich composition of new grains compared to the host porphyroclast.

SED
5, 365–390, 2013



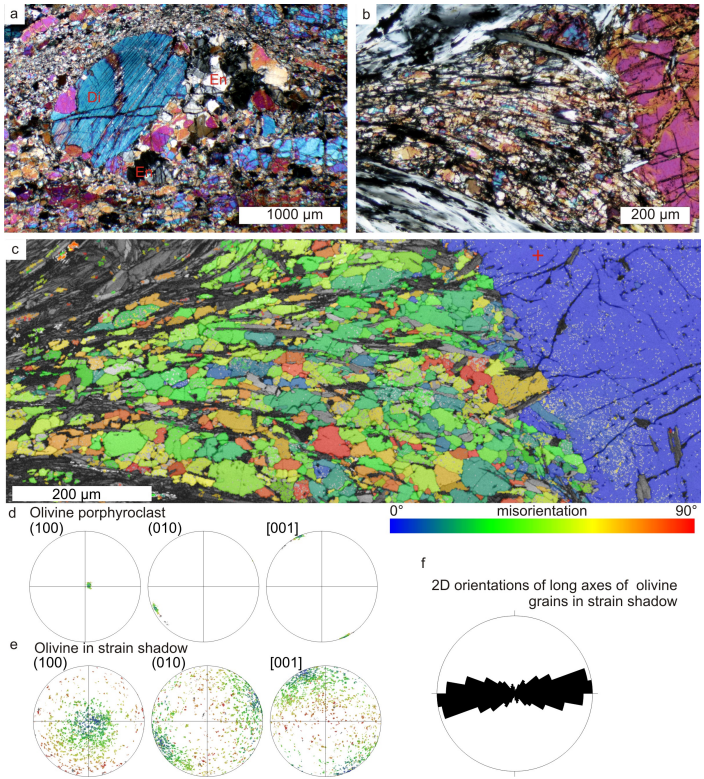


Fig. 6. (a) Optical micrograph (crossed polarizers) showing enstatite (En) in strain shadow around a diopside (Di) porphyroclast (sample CT_07-19). Note that the new pyroxene grains in the strain shadow do not show exsolution lamellae. **(b)** Optical micrograph (crossed polarizers) showing olivine grains in strain shadow around olivine porphyroclast (sample CT_07-14). **(c)** EBSD map and corresponding polefigures of poles to (100), (010) and (001) planes of **(d)** olivine porphyroclast and **(e)** olivine in strain shadow. **(f)** Shape preferred orientation of olivine grains in strain shadow with long axes of grains in the foliation plane.

SED
5, 365–390, 2013



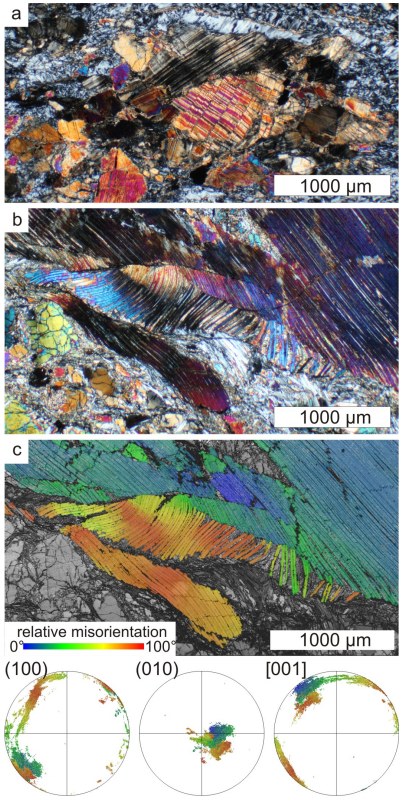


Fig. 7. (a) Optical micrograph (crossed polarizers) showing fractured and bent diopside porphyroclast with exsolution lamellae parallel (100) (sample CT_07-21); **(b)** optical micrograph (crossed polarizers) showing kinked and bent diopside porphyroclast with exsolution lamellae parallel (100) (sample CT_07-13); **(c)** EBSD map (relative misorientation) of kinked and bent diopside porphyroclast of the area shown in b. Corresponding polefigures show dispersed (100) planes and [001] directions. The [010] axis represents the common rotation axis.

SED
5, 365–390, 2013



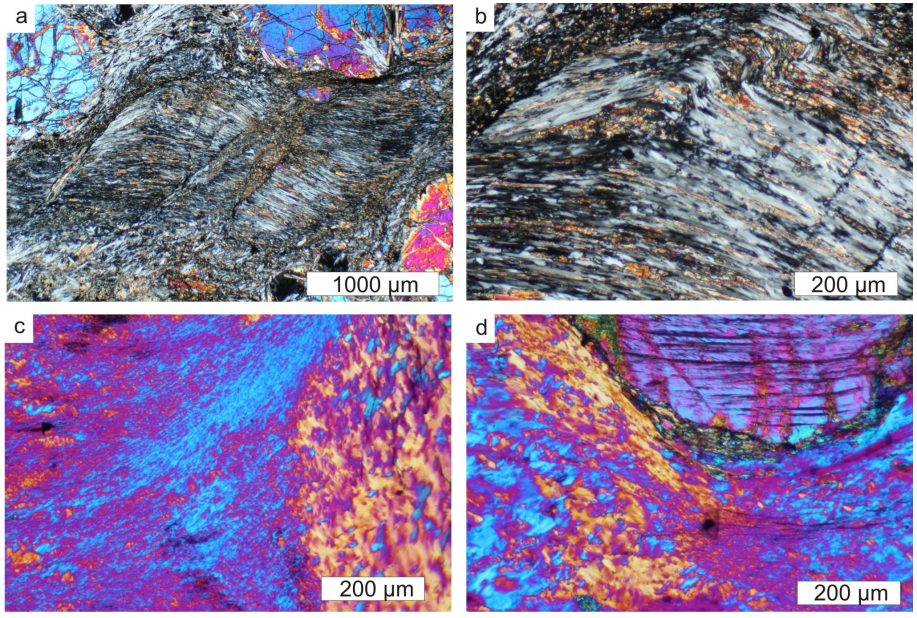


Fig. 8. Optical micrographs (crossed polarizers) showing antigorite microstructures. **(a, b)** Fine-grained antigorite aggregate with strong SPO and CPO forming a crenulation cleavage with olivine present in shear bands (sample CT_07-13). **(c, d)** Fine-grained antigorite aggregates with sutured grain boundaries, SPO and associated CPO deflected around porphyroclasts, photograph taken with λ-compensator plate inserted (sample CT_07-21). Note that the grain size of antigorite is very small at sites of stress concentrations.

SED
5, 365–390, 2013



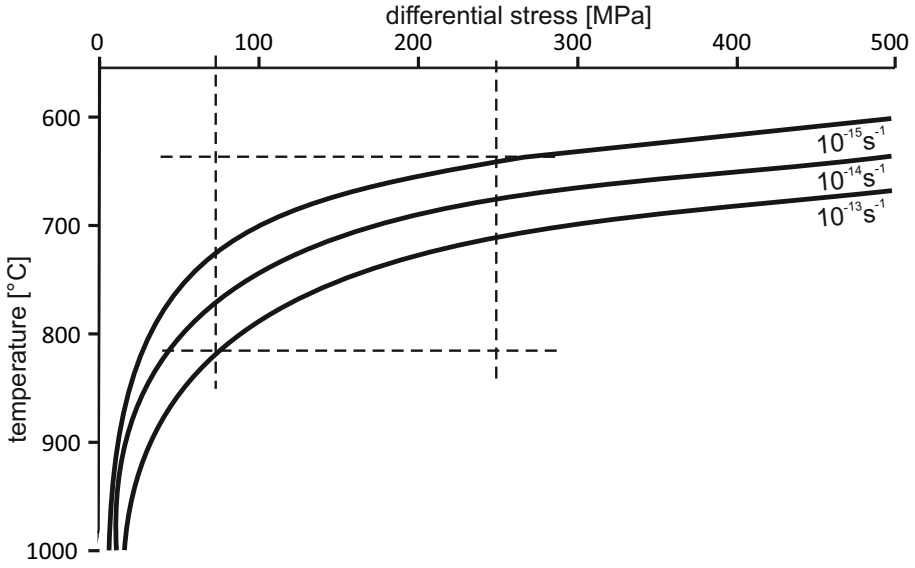


Fig. 9. Flow law for dislocation creep of olivine after Chopra and Paterson (1981).

SED
5, 365–390, 2013

